Experimental Neurology 311 (2019) 285–292

Contents lists available at ScienceDirect

Experimental Neurology

journal homepage: www.elsevier.com/locate/yexnr

Research paper

# Impaired chemoreflex correlates with decreased c-Fos in respiratory brainstem centers of the streptozotocin-induced Alzheimer's disease rat model

Andrea G. Brown[a], Mahima Thapa[b], John W. Hooker IV[b], Tim D. Ostrowski[a,*]

[a] Department of Physiology, Kirksville College of Osteopathic Medicine, A.T. Still University of Health Sciences, Kirksville, MO, USA
[b] Department of Biology, Truman State University, Kirksville, MO, USA

ARTICLE INFO

*Keywords:*
Hypoxia
Respiration
Ventilation
Plethysmography
Nucleus tractus solitarii
Ventral respiratory group
Pre-Bötzinger
Bötzinger
STZ

ABSTRACT

Besides impairment in cognition and memory, patients with Alzheimer's disease (AD) often exhibit marked dysfunction in respiratory control. Sleep-disordered breathing (SDB) is commonly found in cases of AD, resulting in periods of hypoxia during sleep. Early structural changes in brainstem areas controlling respiratory function may account for SDB in the course of AD. However, to date the underlying mechanisms for these complications are not known. The streptozotocin (STZ)-induced rat model of AD exhibits abnormal responses to hypoxia and increased astrogliosis in a key region for respiratory control. In this study we further defined the pathophysiological respiratory response of STZ-AD rats to 10% $O_2$. In addition, we analyzed hypoxia-induced neuronal activation in respiratory and cardiovascular nuclei of the dorsal and ventral brainstem. Two hours of hypoxia induced a transient increase in tidal volume that was followed by a prolonged increase in respiratory rate. Only respiratory rate was significantly blunted in the STZ-AD model, which continued over the entire duration of the hypoxic episode. Analysis of c-Fos expression as a marker for neuronal activation showed abundant labeling throughout the nTS, nuclei of the ventral respiratory column, and A1/C1 cells of cardiovascular centers in the ventral brainstem. STZ-AD rats showed a significant decrease of c-Fos labeling in the caudal/medial nTS, rostral ventral respiratory group, and Bötzinger complex. c-Fos in other respiratory centers and A1/C1 cells was unaltered when compared to control. The results of this study document a region-specific impact of STZ-induced AD in respiratory brainstem nuclei. This decrease in c-Fos expression correlates with the observed blunting of respiration to hypoxia in the STZ-AD rat model.

## 1. Introduction

Alzheimer's disease (AD) is the most common form of dementia and clinically diagnosed largely based on cognitive decline (Alzheimer's Association, 2016; Folstein and Whitehouse, 1983). The majority of AD patients also present with disorders of respiration, swallowing, and autonomic function (Affoo et al., 2013; Engelhardt and Laks, 2008; Femminella et al., 2014; Gaig and Iranzo, 2012). In fact, cardiorespiratory dysfunction is up to 5 times more likely with AD when compared to age-matched controls (Collins et al., 2012; Guo et al., 1996). Sleep-disordered breathing is typically observed in AD patients, with moderate to severe sleep apnea in 30% to 50% of cases, and mild sleep apnea up to 80% of cases (Gaig and Iranzo, 2012; Hoch et al., 1986). Today the mechanisms underlying these respiratory disturbances are not understood.

An important neuronal network controlling normal breathing and responses to hypoxia is situated within the brainstem (Smith et al., 2013). Hypoxia is sensed by peripheral chemoreceptors and centrally integrated in the nucleus tractus solitarii (nTS) (Andresen and Kunze, 1994; Housley et al., 1987). The nTS directly projects to other respiratory centers (e.g. ventral respiratory column), the concerted effort of which ultimately modulates the appropriate response to low-oxygen conditions (i.e. increased ventilation) (Costa et al., 2014). Furthermore, the nTS projects to cardiovascular nuclei in the ventral brainstem (Andresen and Kunze, 1994; Guyenet, 2000) and acute hypoxia increases blood pressure, decreases heart rate, and strengthens respiratory coupling of sympathetic nerve activity (Costa et al., 2014; Moraes et al., 2012). Although AD-related changes of forebrain regions leading to problems with memory and cognition are the prime focus of many studies, AD also affects the integrity of the brainstem (Lee et al., 2015; Parvizi et al., 2001; Simic et al., 2010). Current work suggests that AD pathology in the brainstem manifests simultaneously or even

* Corresponding author at: A.T. Still University of Health Sciences, Kirksville College of Osteopathic Medicine, 800 W. Jefferson St, Kirksville, MO 63501, USA.
*E-mail address:* tostrowski@atsu.edu (T.D. Ostrowski).

https://doi.org/10.1016/j.expneurol.2018.10.012
Received 30 July 2018; Received in revised form 17 September 2018; Accepted 20 October 2018
Available online 23 October 2018

before the changes observed in the forebrain (Lee et al., 2015; Parvizi et al., 2001; Simic et al., 2010). Thus, typical responses to hypoxia may be altered, leading to the sleep-disordered breathing observed in patients with AD.

The streptozotocin (STZ)-induced model of AD mimics many of the typical features of sporadic (95% of cases) AD in humans (Grieb, 2016; Lester-Coll et al., 2006; Rai et al., 2014; Salkovic-Petrisic et al., 2013; Santos et al., 2012). Besides memory dysfunction and astrogliosis in the brain, our laboratory has shown that this model also exhibits significantly blunted chemoreflex responses when exposed to hypoxia (Ebel et al., 2017). This study was a continuation of our previous work and focused on the prolonged respiratory responses to two hours of acute hypoxia (10% $O_2$) and the neuronal activation pattern within specific respiratory and cardiovascular centers in the brainstem of the STZ-AD rat model.

## 2. Materials and methods

### 2.1. Animals

This study used male Sprague-Dawley rats (6–8 weeks) held on a 12-hr day/night cycle at 24 °C and 46% humidity in the AAALAC accredited vivarium of the ATSU Kirksville College of Osteopathic Medicine. Food and water were available ad libitum. Experimental animals were bred in-house from rats purchased from Hilltop Lab Animals or Envigo. Rats were randomly assigned into groups with similar pre-surgical weight (control, $n = 6$, 304.4 ± 23.0 g versus STZ, n = 6, 277.8 ± 31.7 g, $p = .52$). Experimental protocols are approved by the Animal Care and Use Committee of A.T. Still University and in accordance with NIH guidelines ("Guide for the Care and Use of Laboratory Animals").

### 2.2. Induction of the Alzheimer's disease model

Similar to our previous study (Ebel et al., 2017), rats received 1.5 mg/kg streptozotocin (STZ; Alfa Aesar) twice (2 days apart) into the lateral ventricle (bilateral, 5 μL/side). 0.9 mM citrate buffered saline (pH 4.5) served as vehicle. Control animals received vehicle only. For intracerebroventricular (icv) injections, isoflurane-anesthetized animals were positioned in a stereotaxic frame (David Kopf Instruments) and two burr holes were drilled into the skull using a rotary tool (Dremel 7300 with engraving cutter 105). The stereotaxic position of the burr holes and injection site were according to the Paxinos and Watson rat atlas (Paxinos and Watson, 2007): −0.9 mm AP, ± 1.5 mm ML, and 3.6 mm DV. The second icv injection was also performed under isoflurane anesthesia using the same burr holes. STZ and vehicle were injected using glass capillaries (World Precision Instruments) pulled with a micropipette puller (P-97, Sutter Instruments). Rats received 2 mg/kg dexamethasone (immunosuppressant; Auromedics), 50 μg/kg buprenorphine (opioid; Reckitt Benckiser), 7 mg/kg enrofloxacin (antibiotic; Norbrook), and 3 mL 0.9% normal saline (fluid reconstitution; Hospira). The STZ dosage used here was sub-diabetogenic (random blood glucose: vehicle control, $n = 6$, 106.7 ± 3.8 mg/dL versus STZ, $n = 5$, 121.6 ± 10.0 mg/dL, $p = .17$) as determined using a blood glucose tester (TRUEresult, Nipro diagnostics). Following surgery, rats received high sugar supplements (Froot Loops, Kellogg's) in addition to their normal diet to help regain pre-surgical weight.

### 2.3. Assessment of chemoreflex function

Three weeks following final icv injection, conscious unrestrained animals were subjected to acute hypoxia (10% $O_2$, equilibrated with $N_2$) for 2 h in a whole-body flow-through plethysmography chamber (Data Sciences International). Gas supply to the chamber was set at 3 L/min and $O_2/N_2$ ratios controlled using two mass flow controllers (MC-5SLPM-D, Alicat Scientific). Pressure changes within the chamber were recorded with a differential pressure transducer (DP45, Validyne), sine wave carrier demodulator (CD15, Validyne), AD Instruments digitizer (PowerLab 8/35), and LabChart software (AD Instruments). Raw data were analyzed using LabChart and Excel (Microsoft). Respiratory rate, tidal volume, and minute ventilation were averaged from a 30-second segment of calm breathing (in the absence of movements, sniffs, and sighs) at the specified time points. Volume measurements depict the area under the inspiratory pressure curve (ΔP) and were calibrated to pressure changes (ΔPcal) from a known volume of air (Vcal) using a rodent respirator (Harvard Apparatus, Model 680). Tidal volume (TV) was mathematically corrected to accommodate body temperature of the rat (Tb), chamber temperature (Tc), water vapor pressure in the rat (Pw,b) and chamber (Pw,c), and barometric pressure (PB) (Drorbaugh and Fenn, 1955):

$$TV = Vcal \times \frac{\Delta P}{\Delta Pcal} \times \frac{1}{1 - \frac{PB - Pw,b}{PB - Pw,c} \times \frac{Tc}{Tb}}$$

Tidal volume and minute ventilation were furthermore normalized to 100 g of ideal (pre-surgical) rat weight. Ideal rat weight was used due to the significant weight difference between groups at the time of testing (control, $n = 6$, 377.5 ± 17.9 g versus STZ, $n = 6$, 277.7 ± 24.8 g, $p = .004$). Such decrease in weight was likely due to loss of fat mass rather than shrinkage of lung tissue. This hypothesis was validated in a separate set of STZ-injected rats. While post-surgical weight again differed significantly between groups (control, $n = 5$, 362.0 ± 6.2 g versus STZ, $n = 5$, 309.4 ± 19.0 g; $p = .03$), lung tissue weight was similar between vehicle- and STZ-treated rats (wet weight: control, $n = 5$, 1.67 ± 0.04 g versus STZ, n = 5, 1.65 ± 0.19 g, $p = .89$; and dry weight: control, $n = 5$, 0.34 ± 0.01 g versus STZ, n = 5, 0.36 ± 0.04 g, $p = .73$).

### 2.4. Immunohistochemistry

Immediately following the acute hypoxia protocol, all experimental animals were anesthetized with isoflurane and transcardially exsanguinated with heparinized 0.01 M phosphate-buffered saline (PBS; in mM: 2.7 $NaH_2PO_4$, 7.7 $Na_2HPO_4$, and 154 NaCl, pH 7.4). Subsequent fixation was done with 4% paraformaldehyde (PFA; Acros organics) in PBS. The brain was removed, post-fixed over night at 4 °C, and stored in PBS for further processing. 30 μm coronal brainstem sections were cut using a vibrating microtome (7000smz-2, Campden Instruments), and collected/stored in a 24 well-tissue culture plate filled with cryoprotectant (50% PBS, 30% ethylene glycol, and 20% glycerol). A standard protocol was used for immunohistochemical staining (Ebel et al., 2017). Briefly, following washing of sections with PBS, non-specific antibody binding was prevented by blocking 30 min with 10% normal donkey serum (NDS, Millipore) with 0.3% Triton-PBS. Then, sections were incubated in 1% NDS, 0.3% Triton-PBS, and primary antibody on a shaker at room temperature overnight. The primary antibodies used for this study were: c-Fos (goat, 1:500, sc-52G, Santa Cruz), NeuN (rabbit, 1:400, MABN140, Millipore), S100 calcium-binding protein B (S100B; rabbit, 1:200, ab41548, Abcam), and tyrosine hydroxylase (TH; 1:1500, chicken, ab76442, Abcam). Up to three antibodies were used simultaneously in the same tissue. Following primary antibody exposure, sections were washed and incubated in the appropriate secondary antibody for 2 h. All secondary antibodies were used at 1:200 dilution (host: donkey; Alexa Fluor 488, 711-545-152 and 703-545-155; and Alexa Fluor 647, 705-605-147; Jackson Immuno). All sections were mounted on gelatin-coated glass slides, air dried, and cover-slipped using ProLong Diamond (with DAPI; ThermoFisher Scientific). Antibodies were validated in one section by the absence of fluorescence when the primary antibody was omitted.

Immunofluorescence was visualized with appropriate filter sets using an epifluorescent microscope (Eclipse 80i, Nikon) and digital monochrome camera (DS-Qi1Mc, Nikon). Identical exposure times

between treatment groups allowed comparison of staining intensity and the same intensity threshold counting criteria for faintly stained cells. Post-processing of the images was done using Fiji (Version 1.52d, NIH). Some images were stitched using the Fiji plugin *MosaicJ* (Thévenaz and Unser, 2007). Templates were drawn according to our brain sections with the program Inkscape (version 0.91; http://www.inkscape.org/) and nuclei identified with the help of Paxinos & Watson rat brain atlas (Paxinos and Watson, 2007). The distinction between adjacent respiratory and cardiovascular nuclei (C1 and A1/C1 region) in the ventral brainstem was based on our templates individually adjusted to prominent structures in the section, including the clearly visible nucleus ambiguus, ventral part of the spinal trigeminal tract, pyramidal tract and inferior olive, as well as dorsal aspects such as the hypoglossal nucleus and nTS. Furthermore, in some sections we verified the accuracy of our templates by double-labeling of c-Fos and TH. Sections were counted in a blinded fashion by four independent persons and results were averaged. Most animals were accustomed to the plethysmography chamber for 1 h on each of the two days before testing. In one experimental run, however, two rats from each group were exposed to acute hypoxia without prior acclimatization to the chamber, which resulted in increased c-Fos expression when compared to all other animals tested. Thus, before averaging, c-Fos counts were normalized to the section with the highest number of stained cells (set to 1) within an experimental run (2 STZ and 2 CTL rats per run). Cell nuclei stained with DAPI were counted in a 150 × 150 μm box in the nTS with the highest density of c-Fos labeling. Increased c-Fos labeling was usually found in the medial dorsal-most region of each nTS hemi-section. Areas devoid of cells, such as blood vessels or nucleus borders were avoided.

### 2.5. Statistical analysis

SigmaPlot 14.0 (Systat Software) was used for all statistical analysis. Respiratory parameters and immunohistochemical data from the nTS were compared between groups using 2-way repeated ANOVA with Student-Newman-Keuls post hoc test. Changes of respiratory and c-Fos data from ventral brainstem nuclei were analyzed using *t*-tests. Results were considered statistically significant with $p$ values $\leq .05$. Group data are presented as mean ± standard error of the mean.

## 3. Results

### 3.1. STZ-AD rats exhibit a sustained blunted chemoreflex response to hypoxia

Rats exposed to 10% $O_2$ showed peripheral chemoreflex modulation of breathing with a notable increase in respiratory rate (Fig. 1A). In addition, sighs (augmented breaths to re-open collapsed alveoli) were observed more frequently under low oxygen conditions (large excursion in Fig. 1A *bottom*). Over the course of 2 h of hypoxia, the increase in respiratory rate peaked after ~5–10 min and remained elevated (although at a lower level) throughout the entire hypoxic exposure (Fig. 1B *upper trace*). This initial peak of respiratory rate was strongly diminished in the STZ-AD rat model (Fig. 1B *lower trace*). The decreased response to hypoxia was also evident throughout the entire hypoxic period. Respiratory rate towards the end of the hypoxic protocol was only slightly higher than that under normoxic conditions (beginning of the lower trace in Fig. 1B).

The group data confirm that the initial chemoreflex-mediated increase in minute ventilation was significantly blunted in STZ-AD rats 5 min into the hypoxic period (Fig. 2A*left* & *middle*). While minute ventilation in control rats increased by 107%, STZ-AD rats exhibited only a 64% increase in response to hypoxia. These results are similar to those from our previous study using short exposures to various levels of hypoxia (Ebel et al., 2017). Additionally, following the peak increase at 5 min, minute ventilation remained elevated in control rats throughout the entire period of hypoxia (Fig. 2A *right*) with a minimal elevation of minute ventilation of 43% (at 90 min) from the initial value at normoxia (at 0 min). In contrast, STZ-AD rats displayed continued blunting of the chemoreflex response with a minimal elevation of 16% (at 90 min). A closer look at tidal volume and respiratory rate shows that changes in minute ventilation of STZ-AD rats were entirely due to a blunted increase in breathing rate (Fig. 2B). Interestingly, both rat groups showed an early hypoxia-induced increase in tidal volume (at 5 min). This increase in tidal volume, however, quickly returned to baseline while respiratory rate had a delayed peak after 10 min of hypoxia. These data suggest that sudden changes in lung oxygenation may be primarily compensated by instantaneous changes in tidal volume, and that longer episodes of hypoxia may be primarily compensated by changes in respiratory rate.

### 3.2. Reduced hypoxia-mediated c-Fos labeling of caudal/medial nTS neurons in STZ-AD rats

To identify the possible underlying cause for diminished chemoreflex activation in the STZ-AD model, rat brains were paraformaldehyde-fixed immediately following the hypoxic episode for immunohistochemical analysis. We first examined cellular activation (as indicated by c-Fos staining (Dragunow and Faull, 1989)) in the nucleus tractus solitarii (nTS), the initial central nucleus in the peripheral chemoreflex axis. A representative staining of a control and STZ-AD rat

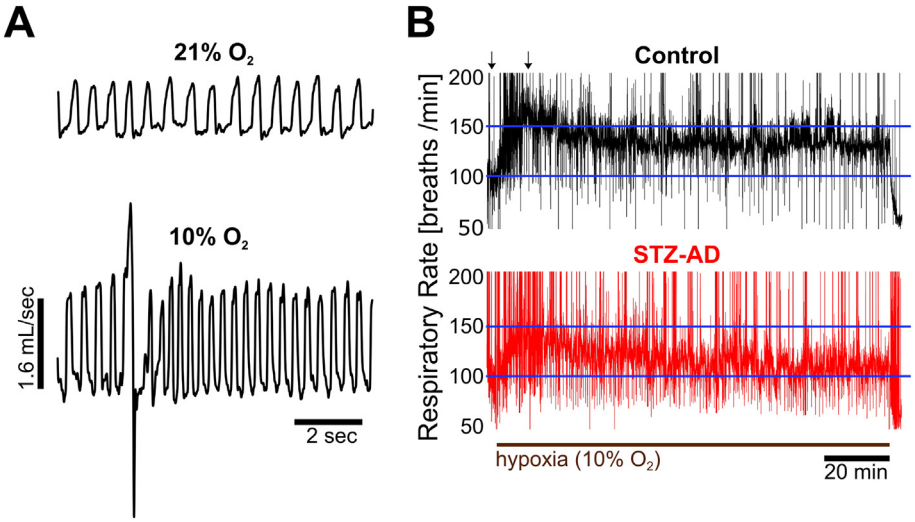


**Fig. 1.** Respiratory responses of control and STZ-AD rats to hypoxia. A) Typical respiratory recordings during normoxia and 10% $O_2$. Upward movement = inspiration. B) Examples for respiratory rate over 2 h 10% $O_2$ from a control (*top*) and streptozotocin-induced Alzheimer's disease (STZ-AD) rat (*bottom*). Note the blunted increase of respiratory rate in STZ-AD. Arrows indicate the time points for the examples shown in A. Large excursions (noise) are from sniffing or rat movements in the plethysmography chamber.

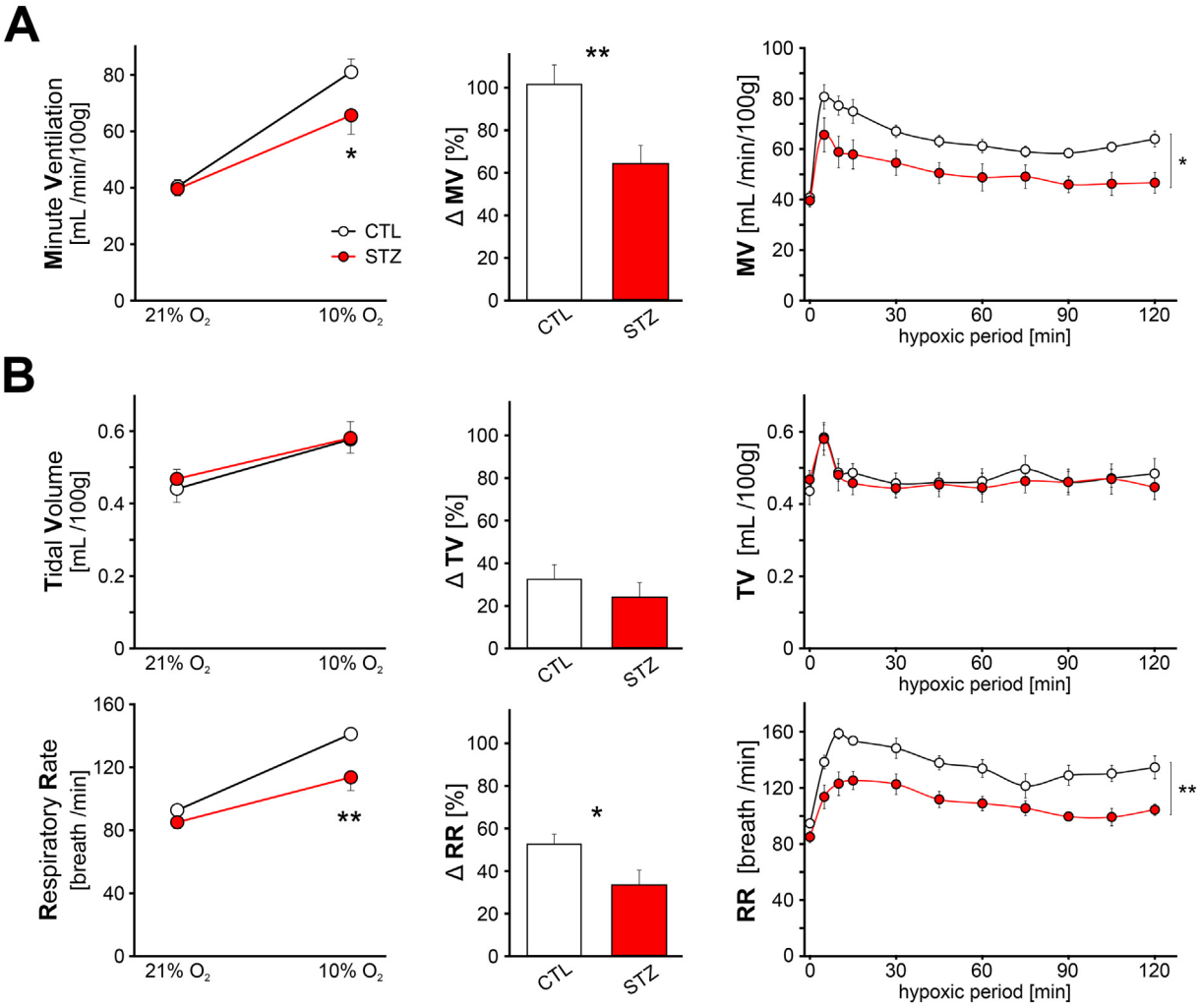


**Fig. 2.** Group data for respiratory parameters showing decreased peripheral chemoreflex response in STZ-AD. A) Minute ventilation (MV) normalized to 100 g rat at 5 min (*left*), the change from normoxia to hypoxia (*middle*), and long-term MV over 2 h (*right*) for control (CTL) and STZ-AD. B) Breakdown of MV data (shown in A) into tidal volume (TV) and respiratory rate (RR) for CTL and STZ-AD. Note the transient increase in TV and prolonged increase of RR. * $p \leq .05$, ** $p \leq .01$. $n = 6$ for each group.

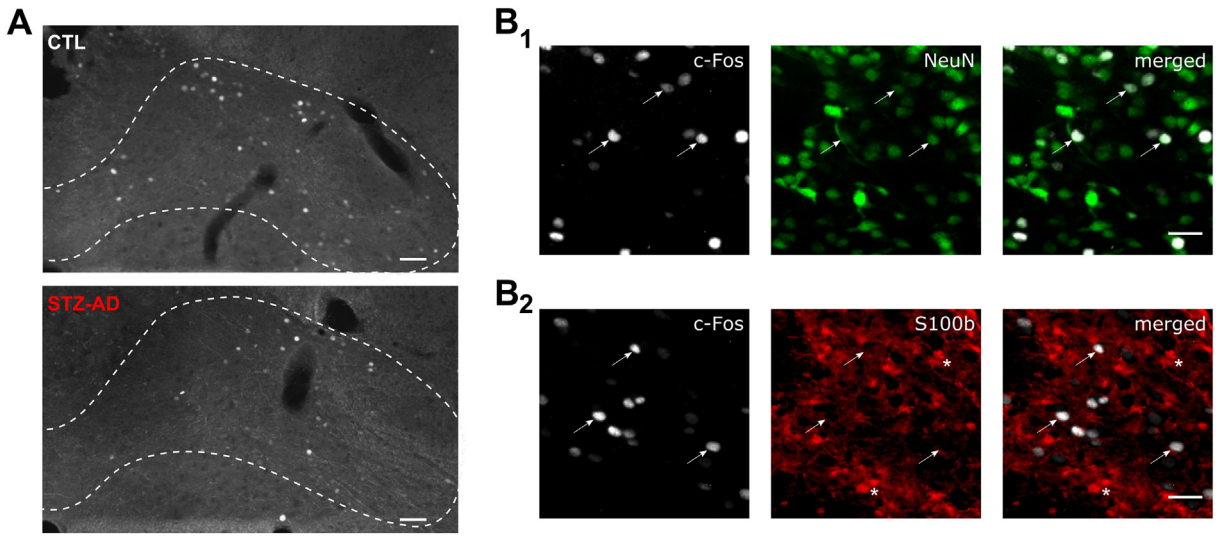


**Fig. 3.** c-Fos labeling in nTS neurons of control and STZ-AD rats following 2 h of hypoxia. A) Representative example of hypoxia-induced c-Fos (cell activity marker) labeling in the nucleus tractus solitarii of control (CTL; *top*) and streptozotocin-induced Alzheimer's disease (STZ-AD, *bottom*). Scale = 100 μm. $B_1$) Double-labeling of c-Fos and NeuN (neuronal marker). Arrows point towards c-Fos labeled nuclei that co-labeled with NeuN. Scale = 50 μm. $B_2$) Double-labeling of c-Fos and S100b (astroglial marker). Arrows point towards c-Fos labeled nuclei that were devoid of S100b. Stars indicate position of an astroglial cell body. Scale = 50 μm.

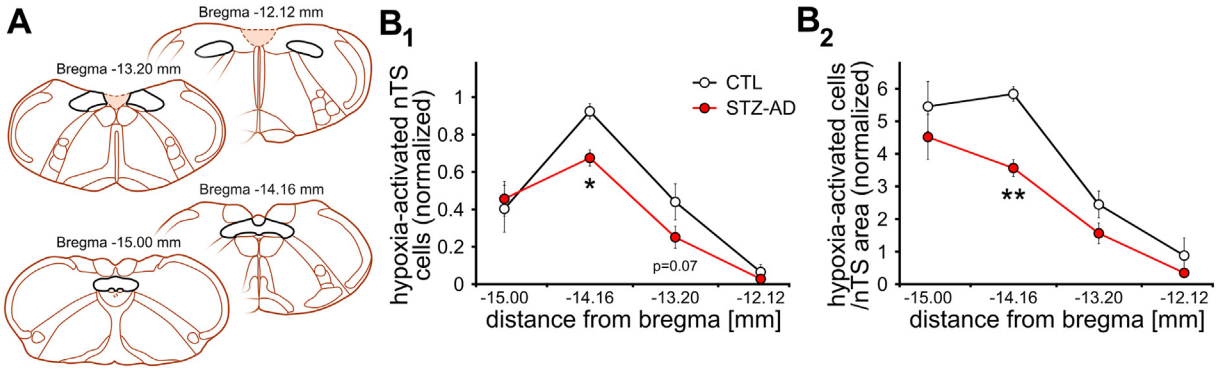


**Fig. 4.** Group data showing decreased hypoxia-induced c-Fos labeling in the caudal/medial nTS of STZ-AD rats. A) Coronal templates depicting the positions (from bregma according to Paxinos and Watson) for bilateral quantification of c-Fos within the rostral-caudal extent of the nucleus tractus solitarii (nTS). Bold line depicts the extent of the nTS. $B_1$) Average group data for c-Fos expression in control (CTL) and streptozotocin-induced Alzheimer's disease (STZ-AD) at the four nTS levels shown in A. Data is normalized to the maximum number of c-Fos labeled cells (= 1) within an experimental run (see Materials & Methods). $B_2$) Group data shown in B1 is normalized to nTS area. * $p \leq .05$, ** $p \leq .01$. n = 6 for each group.

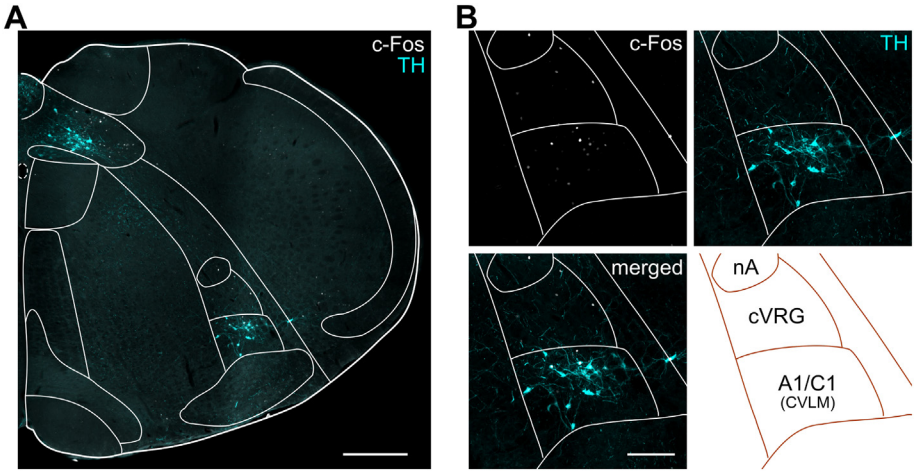


**Fig. 5.** c-Fos labeling in respiratory and cardiovascular regions of the ventral brainstem in control and STZ-AD following 2 h of hypoxia. A) Overview section with template overlay (Bregma −14.16 mm) indicating c-Fos (*white*) and tyrosine hydroxylase (TH; *cyan*). Scale = 500 µm. B) Zoom on c-Fos expressing cells in the caudal ventral respiratory group (cVRG) and A1/C1 cell group that co-labels with TH. The A1/C1 group is located at the level of the caudal ventrolateral medulla (CVLM). nA = nucleus ambiguus. Scale = 300 µm. (For interpretation of the references to color in this figure legend, the reader is referred to the web version of this article.)

is shown in Fig. 3A. Two hours of acute hypoxia consistently elicited c-Fos staining in both rat groups throughout the entire extent of the nTS. Similar to other studies (Gozal et al., 1999), we verified in a few sections that cell activation is largely found in NeuN-identified neurons (Fig. 3$B_1$). On the other hand, c-Fos was absent in S100b-identified astrocytes (Fig. 3$B_2$).

Quantitatively we analyzed cellular activation in 4 representative sections throughout the extent of the nTS (Fig. 4A). Using landmarks in the brainstem section and the Paxinos & Watson rat brain atlas (Paxinos and Watson, 2007), nTS regions evaluated correspond to the commissural nTS (Bregma −15.00 mm), caudal/medial nTS (Bregma −14.16), medial nTS (Bregma −13.20 mm), and rostral nTS (Bregma −12.12 mm). A maximum number of c-Fos labeled cells was found in the caudal/medial nTS (Bregma −14.16) of both groups (Fig. 4$B_1$; cell counts were normalized to the highest cell count in an experimental run - see Materials & Methods; averaged maximum of all runs was 143 ± 28.5 c-Fos labeled cells). However, in this section of the nTS there was significantly less c-Fos labeling in STZ-AD rats. A reduced hypoxia-induced activation of the nTS may in part explain the observed chemoreflex dysfunction of this AD model.

It has been previously shown that brain mass, especially in the hippocampal region, decreases in AD patients (Kesslak et al., 1991; Zimny et al., 2013). Similarly, cerebral atrophy is found in the STZ-AD rat model (Kraska et al., 2012; Shoham et al., 2003). To account for potential errors introduced by overall nTS size, c-Fos counts were normalized to the area evaluated (Fig. 4$B_2$). Normalizing to nTS size showed highest hypoxia-mediated activation in the caudal-most sections. Again, neuronal activation was significantly lower in the caudal/medial nTS of STZ-AD rats. To examine the possibility that a decrease in cell number may account for the lower c-Fos labeling observed in STZ-AD rats, DAPI-stained cell nuclei were counted bilaterally in a 150 × 150 µm box placed in areas of highest cellular activation from hypoxia. However, there was no statistical difference between both experimental groups in overall cell number (sum of all four nTS sections: control, $n = 6$, 458.2 ± 9.5 versus STZ, $n = 6$, 478.8 ± 17.6, $p = .33$). There was also no regional difference of cell number in the rostral-caudal extent of nTS sections analyzed (data not shown). These results indicate that decreased c-Fos labeling in the STZ-AD rat is not due to a decrease in overall cell number.

### 3.3. Reduced hypoxia-induced c-Fos labeling in the rostral VRG and Bötzinger complex in STZ-AD rats

We furthermore analyzed potential changes in neuronal activation within respiratory centers of the ventral brainstem. Since these respiratory nuclei are directly adjacent (dorsal) to cardiovascular centers, we verified the accuracy of our templates in some animals using double-labeling of c-Fos and tyrosine hydroxylase (TH; Fig. 5). TH was primarily found in neurons of the A1 and C1 cell group and thus distinguished these cells from TH-negative neurons in respiratory centers of the ventral brainstem (Kanjhan et al., 1995; Verberne et al., 1999; Wang et al., 2001). We only observed very sparse hypoxia-induced c-Fos labeling in respiratory nuclei, while there was strong staining in cardiovascular nuclei (Fig. 5B). This result is consistent with data

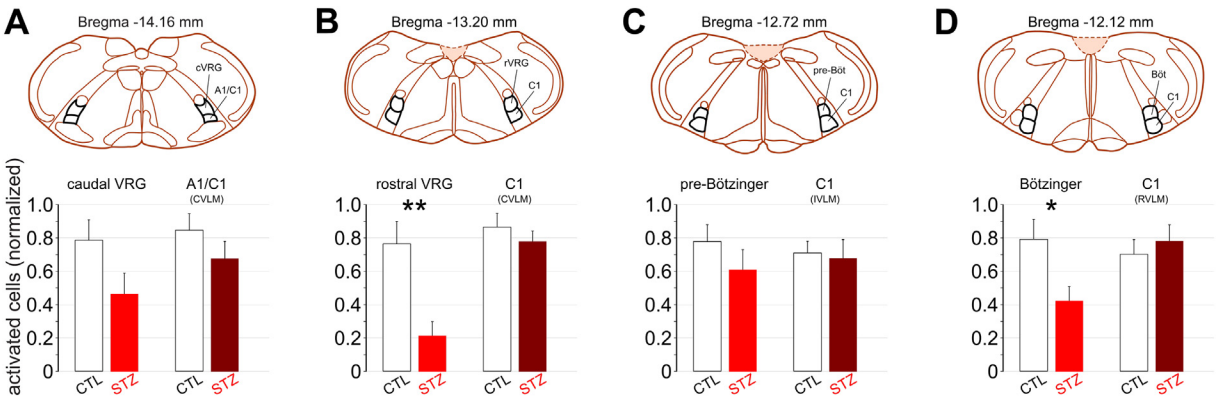


**Fig. 6.** Averaged group data showing decreased hypoxia-induced c-Fos with STZ-AD in specific respiratory nuclei of the ventral brainstem. A) Orientation template (*top*) and c-Fos data (*bottom*; normalized to maximum c-Fos count per experimental run - see Materials & Methods) in the caudal ventral respiratory group (cVRG) and A1/C1 cell group (caudal ventrolateral medulla [CVLM] region). $n = 6$ for control (CTL) and $n = 5$ for streptozotocin (STZ)-induced Alzheimer's disease. B) Template and c-Fos in the rostral ventral respiratory group (rVRG) and C1 cell group (CVLM region). $n = 6$ for each group. C) Template and c-Fos in the pre-Bötzinger (pre-Böt) and C1 cell group (intermediate ventrolateral medulla [IVLM] region). $n = 6$ for each group. D) Template and c-Fos in the Bötzinger (Böt) and C1 cell group (rostral ventrolateral medulla [RVLM] region). * $p \leq .05$, ** $p \leq .01$. n = 6 for each group.

published previously by others (King et al., 2013; Wang et al., 2015).

We quantified c-Fos labeling in the caudal and rostral extent of the ventral respiratory group (VRG), the pre-Bötzinger complex, the Bötzinger complex, as well as in adjacent regions important for cardiovascular function (A1 and C1 cell groups; Fig. 6). Regions were aligned with the Paxinos and Watson rat brain atlas (Paxinos and Watson, 2007) and approximately subdivided into caudal, intermediate, and rostral portions of the ventrolateral medulla (Horiuchi et al., 1999) as shown in the figure. There was no difference in any of the cardiovascular regions analyzed between both experimental groups (maximum average c-Fos labeled cell count of all runs: A1/C1 (Fig. 6A), 38 ± 8.2 cells; C1 (Fig. 6B), 38 ± 5.5 cells; C1 (Fig. 6C), 39 ± 1.0 cells; C1 (Fig. 6D), 35 ± 1.6 cells). Thus, although cardiovascular nuclei exhibited strong c-Fos labeling after two hours of acute hypoxia, STZ-induced AD had no impact on the activation pattern in these regions. In regards to the respiratory nuclei, there was no change in cell activation in the caudal VRG and pre-Bötzinger complex of the STZ-AD rat model (maximum average c-Fos: cVRG, 13 ± 3.0 cells; pre-Bötzinger, 9 ± 1.1 cells). However, c-Fos labeling was significantly lower in the rostral VRG (maximum average c-Fos: 15 ± 2.1 cells) and Bötzinger complex (maximum average c-Fos: 10 ± 1.9 cells) of STZ-AD rats when compared to control. Decreased hypoxia-induced cell activation in these regions may furthermore contribute to the observed blunting of peripheral chemoreflex responses in STZ-AD rats.

## 4. Discussion

Here we show for the first time a long-term diminution of hypoxia-induced chemoreflex activation in the STZ-AD rat model. The pronounced reduction of minute ventilation continued over our entire recording period of 2 h and was entirely due to a blunted increase of respiratory rate. Immunohistochemical analysis of brainstem centers important for respiratory control identified novel target regions impacted by STZ-AD. Particularly the caudal/medial nTS exhibited a significant decrease of hypoxia-induced cell activation. This decrease in c-Fos labeling was not due to an overall decrease in cell number. Furthermore, the rostral VRG and the Bötzinger complex showed reduced c-Fos staining, whereas adjacent ventral respiratory (caudal VRG & pre-Bötzinger complex) and cardiovascular (A1/C1 cells) nuclei were unaltered.

It is widely documented that, amongst many other physiological functions, the nTS plays an important role in normal respiratory function (Andresen and Kunze, 1994; Braccialli et al., 2008; Housley and Sinclair, 1988). Furthermore, it is the first central integration point in the peripheral chemoreflex arc and thus of high importance for adequate responses to hypoxic conditions (Favero et al., 2011). Our study showed that hypoxia-induced neuronal activation in the nTS is diminished in the STZ-AD model. A significantly decreased c-Fos expression has also been observed in hippocampal brain regions of this model following behavioral tests for long-term memory formation (Jee et al., 2008). At this point, the exact reason for decreased c-Fos expression in the STZ-AD rats is not clear, but it seems not to be due to a general reduction in cell number (as shown by our DAPI analysis). Lower c-Fos staining may be due to local impairment of neuronal energy metabolism (Nitsch and Hoyer, 1991). Dysregulation of brain glucose and desensitization of neuronal insulin receptors has been previously shown to occur in the STZ-AD model (Correia et al., 2011; Lester-Coll et al., 2006). These pathologic processes also occur in patients with AD (La Monte and Wands, 2005). On the other hand, both AD in human and STZ-induced AD in rats are strongly associated with increased levels of inflammation and oxidative stress (Berr et al., 2000; Cervellati et al., 2013; Griffin et al., 1989; Rai et al., 2014; Sharma and Gupta, 2001). These factors mostly contribute to neuronal hyperexcitability in the nTS as shown by electrophysiological studies (Emch et al., 2000; Marty et al., 2008; Ostrowski et al., 2017; Ostrowski et al., 2014; Pickering et al., 2005). A potential increase of overall neuronal activity in the nTS of STZ-AD rats may mask hypoxia-induced c-Fos expression, since the transiently expressed c-Fos protein decreases to baseline levels with prolonged cellular activity (Hope et al., 1992). Potential basal hyperexcitation in respiratory nuclei may furthermore contribute to a “ceiling effect” response, in which neurons are not capable of coding stronger stimuli via increased spiking when e.g. stimulated by hypoxia. This ceiling effect, in turn, may then present as the blunted chemoreflex observed in this study. Future analysis of neurophysiological properties in the nTS of STZ-AD rats will answer this question.

Extensive research focused on the functional roles of sub-nuclei within the ventral respiratory column (VRC) (Abdala et al., 2009; Costa et al., 2014; Monnier et al., 2003; Smith et al., 2013). Similar to others (Teppema et al., 1997; Wang et al., 2015), we have found c-Fos labeling throughout the VRC regions analyzed in this study, confirming peripheral chemoreflex activation of these nuclei and their role in the hypoxic response. The number of c-Fos stained cells, however, is likely underestimated due to our strict template-determined boundaries (aided by double-labeling against TH, see Materials and Methods) between respiratory nuclei and A1/C1 cell clusters. This method may have excluded a portion of c-Fos-positive respiratory cells that were intermingled within groups of TH-positive cells, and is a limitation of the present study. Nevertheless, in the group of c-Fos labeled cells that

were associated with respiratory nuclei, we observed significantly decreased cell activation in response to hypoxia in the rostral VRG and Bötzinger complex of STZ-AD rats. At this point it is not clear if reduced c-Fos labeling in these ventral respiratory nuclei is merely due to reduced activation in the nTS (i.e. reduced activity in the nTS leads to reduced activity in subsequent nuclei), or whether the action of STZ is region-specific and independent from that observed in the nTS.

While activity of the rostral VRG and pre-Bötzinger complex is required during inspiration, activation of the caudal VRG and Bötzinger complex becomes important during expiration (Smith et al., 2013). The impact of these sub-regions on respiratory rate has been previously defined by local injections of a glutamate receptor agonist (Bonham and Jeske, 1989; Monnier et al., 2003). While injections into the pre-Bötzinger complex produced tachypnea, respiratory rate deceased with activation of the rostral VRG or Bötzinger complex. The opposite (bradypnea) seems true with local injections of glutamate receptor blockers in the rostral VRG and Bötzinger complex (Anderson and Speck, 1999; Moraes et al., 2012; Mutolo et al., 2005). While these data for pre-Bötzinger (inspiratory rhythm generator) and Bötzinger complex (expiratory control) seem consistent with their functional role in respiration, changes in respiratory rate with microinjections into the rostral VRG (mainly inspiratory pre-motor neurons) seem unexpected and opposite in relation to the prospective function (Smith et al., 2013). The authors speculate that their findings may be based on changes in the activity of inhibitory sub-populations in this nucleus, synchronizing firing of neuronal populations that normally fire out of phase, or induction of supernormal discharge rates with glutamate receptor agonists (Bonham and Jeske, 1989; Monnier et al., 2003). Irrespective of the underlying mechanism, one may conclude from these studies that lower activation (similar to local blockage) of the rostral VRG and Bötzinger complex in the STZ-AD model could potentially lead to exaggerated responses to hypoxia. Such an assumption, however, is in contrast to the observed blunting of respiratory rate in STZ-AD rats during hypoxia. Alternatively, chronic neuronal hyperactivity in these nuclei (and a masking of c-Fos expression, see above) would be in line with the findings from glutamate receptor activation in the VRC.

The cardiovascular network in the ventral brainstem (CVLM, IVLM, and RVLM) is mainly associated with the classical baroreflex (Dampney et al., 2003; Schreihofer and Guyenet, 2002). Similar to others (Guyenet, 2000; King et al., 2013; Teppema et al., 1997), we observed strong activation of cardiovascular nuclei with 10% $O_2$, indicating their role during hypoxia-induced changes in cardiovascular function. While the exact neuronal pathways for chemoreflex-mediated sympathoactivation and cardiovascular responses are still not entirely understood, direct and indirect projections from the nTS to the RVLM and ventrolateral pons (A5 cell group) seem to play an essential role (Guyenet and Koshiya, 1995). CVLM neurons, on the other hand, rather modulate sympathetic responses to acute hypoxia (Mandel and Schreihofer, 2009). However, c-Fos immunoreactivity in A1/C1 cells of STZ-AD rats was not altered when compared to control animals. This result may be indicative of unaltered cardiovascular responses to hypoxia in STZ-AD rats. Future studies need to clarify the potential physiological alterations of the cardiovascular system to hypoxia, and whether STZ induces structural/cellular changes in the nuclei controlling these functions.

In conclusion, we have shown a significant reduction of the chemoreflex-mediated respiratory response to 2 h of acute hypoxia in the STZ-AD rat model. These results correlate with decreased c-Fos expression in respiratory nuclei of the brainstem (nTS, rostral VRG, and Bötzinger complex). On the other hand, c-Fos labeling in other regions typically activated by hypoxia (pre-Bötzinger complex, caudal VRG, and A1/C1 cells) remained unchanged. Such region-specific reduction of c-Fos gives important new insights about the affected respiratory nuclei in STZ-AD rats, and contributes to an explanation for the blunted respiratory response to hypoxia in this model.

## Acknowledgments

We thank Dr. D.S. Middlemas for the provision of the microscope for immunohistochemical analysis. This study was supported with work study money (to AGB) and seed money (to TDO) from ATSU KCOM.

## References

Abdala, A.P.L., Rybak, I.A., Smith, J.C., Paton, J.F.R., 2009. Abdominal expiratory activity in the rat brainstem-spinal cord in situ: patterns, origins and implications for respiratory rhythm generation. J. Physiol. 587, 3539–3559. https://doi.org/10.1113/jphysiol.2008.167502.

Affoo, R.H., Foley, N., Rosenbek, J., Shoemaker, J.K., Martin, R.E., 2013. Swallowing dysfunction and autonomic nervous system dysfunction in Alzheimer's disease: a scoping review of the evidence. J. Am. Geriatr. Soc. 61, 2203–2213. https://doi.org/10.1111/jgs.12553.

Alzheimer's Association, 2016. 2016 Alzheimer's disease facts and figures. Alzheimers Dement. 12, 459–509. https://doi.org/10.1016/j.jalz.2015.02.003.

Anderson, M.K., Speck, D.F., 1999. Differential effects of excitatory amino acid receptor antagonism in the ventral respiratory group. Brain Res. 829, 69–76.

Andresen, M.C., Kunze, D.L., 1994. Nucleus tractus solitarius-gateway to neural circulatory control. Annu. Rev. Physiol. 56, 93–116. https://doi.org/10.1146/annurev.ph.56.030194.000521.

Berr, C., Balansard, B., Arnaud, J., Roussel, A.M., Alpérovitch, A., 2000. Cognitive decline is associated with systemic oxidative stress: the EVA study. Etude du Vieillissement Artériel. J. Am. Geriatr. Soc. 48, 1285–1291. https://doi.org/10.1111/j.1532-5415.2000.tb02603.x.

Bonham, a C., Jeske, I., 1989. Cardiorespiratory effects of DL-homocysteic acid in caudal ventrolateral medulla. Am. J. Phys. 256, H688–H696. https://doi.org/10.1152/ajpheart.1989.256.3.H688.

Braccialli, A.L., Bonagamba, L.G.H., Machado, B.H., 2008. Glutamatergic and purinergic mechanisms on respiratory modulation in the caudal NTS of awake rats. Respir. Physiol. Neurobiol. 161, 246–252. https://doi.org/10.1016/j.resp.2008.02.011.

Cervellati, C., Cremonini, E., Bosi, C., Magon, S., Zurlo, A., Bergamini, C.M., Zuliani, G., 2013. Systemic oxidative stress in older patients with mild cognitive impairment or late onset Alzheimer's disease. Curr. Alzheimer Res. 10, 365–372. https://doi.org/10.2174/1567205011310040003.

Collins, O., Dillon, S., Finucane, C., Lawlor, B., Kenny, R.A., 2012. Parasympathetic autonomic dysfunction is common in mild cognitive impairment. Neurobiol. Aging 33, 2324–2333. https://doi.org/10.1016/j.neurobiolaging.2011.11.017.

Correia, S.C., Santos, R.X., Perry, G., Zhu, X., Moreira, P.I., Smith, M.A., 2011. Insulin-resistant brain state: the culprit in sporadic Alzheimer's disease? Ageing Res. Rev. 10, 264–273. https://doi.org/10.1016/j.arr.2011.01.001.

Costa, K.M., Accorsi-Mendonça, D., Moraes, D.J.A., Machado, B.H., 2014. Evolution and physiology of neural oxygen sensing. Front. Physiol. 5, 1–16. https://doi.org/10.3389/fphys.2014.00302.

Dampney, R.A.L., Polson, J.W., Potts, P.D., Hirooka, Y., Horiuchi, J., 2003. Functional organization of brain pathways subserving the baroreceptor reflex: studies in conscious animals using immediate early gene expression. Cell. Mol. Neurobiol. 23, 597–616. https://doi.org/10.1023/A:1025080314925.

Dragunow, M., Faull, R., 1989. The use of c-fos as a metabolic marker in neuronal pathway tracing. J. Neurosci. Methods 29, 261–265.

Drorbaugh, J.E., Fenn, W.O., 1955. A barometric method for measuring ventilation in newborn infants. Pediatrics 16, 81–87.

Ebel, D.L., Torkilsen, C.G., Ostrowski, T.D., 2017. Blunted respiratory responses in the streptozotocin-induced Alzheimer's disease rat model. J. Alzheimers Dis. 56, 1197–1211. https://doi.org/10.3233/JAD-160974.

Emch, G.S., Hermann, G.E., Rogers, R.C., 2000. TNF-alpha activates solitary nucleus neurons responsive to gastric distension. Am. J. Physiol. Gastrointest. Liver Physiol. 279, G582–G586.

Engelhardt, E., Laks, J., 2008. Alzheimer disease neuropathology: understanding autonomic dysfunction. Dement. Neuropsychol. 2, 183–191.

Favero, M.T., Takakura, A.C., de Paula, P.M., Colombari, E., Menani, J.V., Moreira, T.S., 2011. Chemosensory control by commissural nucleus of the solitary tract in rats. Respir. Physiol. Neurobiol. 179, 227–234. https://doi.org/10.1016/j.resp.2011.08.010.

Femminella, G.D., Rengo, G., Komici, K., Iacotucci, P., Petraglia, L., Pagano, G., de Lucia, C., Canonico, V., Bonaduce, D., Leosco, D., Ferrara, N., 2014. Autonomic dysfunction in Alzheimer's disease: tools for assessment and review of the literature. J. Alzheimers Dis. 42, 369–377. https://doi.org/10.3233/JAD-140513.

Folstein, M., Whitehouse, P., 1983. Cognitive impairment of alzheimer disease. Neurobehav.Toxicol.Teratol. 5, 631–634.

Gaig, C., Iranzo, A., 2012. Sleep-disordered breathing in neurodegenerative diseases. Curr. Neurol. Neurosci. Rep. 12, 205–217. https://doi.org/10.1007/s11910-011-0248-1.

Gozal, D., Xue, Y.D., Simakajornboon, N., 1999. Hypoxia induces c-Fos protein expression in NMDA but not AMPA glutamate receptor labeled neurons within the nucleus tractus solitarii of the conscious rat. Neurosci. Lett. 262, 93–96. https://doi.org/10.1016/S0304-3940(99)00065-8.

Grieb, P., 2016. Intracerebroventricular streptozotocin injections as a model of Alzheimer's disease: in search of a relevant mechanism. Mol. Neurobiol. 53, 1741–1752. https://doi.org/10.1007/s12035-015-9132-3.

Griffin, W.S., Stanley, L.C., Ling, C., White, L., MacLeod, V., Perrot, L.J., White, C.L.,

Araoz, C., 1989. Brain interleukin 1 and S-100 immunoreactivity are elevated in down syndrome and alzheimer disease. Proc. Natl. Acad. Sci. U. S. A. 86, 7611–7615. https://doi.org/10.1073/pnas.86.19.7611.

Guo, Z., Viitanen, M., Fratiglioni, L., Winblad, B., 1996. Low blood pressure and dementia in elderly people: the Kungsholmen project. BMJ 312, 805–808. https://doi.org/10.1136/bmj.312.7034.805.

Guyenet, P.G., 2000. Neural structures that mediate sympathoexcitation during hypoxia. Respir. Physiol. 121, 147–162. https://doi.org/10.1016/S0034-5687(00)00125-0.

Guyenet, P.G., Koshiya, N., 1995. Working model of the sympathetic chemoreflex in rats. Clin. Exp. Hypertens. 17, 167–179.

Hoch, C.C., Reynolds, C.F., Kupfer, D.J., Houck, P.R., Berman, S.R., Stack, J.A., 1986. Sleep-disordered breathing in normal and pathologic aging. J. Clin. Psychiatry 47, 499–503.

Hope, B., Kosofsky, B., Hyman, S.E., Nestler, E.J., 1992. Regulation of immediate early gene expression and AP-1 binding in the rat nucleus accumbens by chronic cocaine. Proc. Natl. Acad. Sci. U. S. A. 89, 5764–5768. https://doi.org/10.1073/pnas.89.13.5764.

Horiuchi, J., Potts, P.D., Polson, J.W., Dampney, R.A., 1999. Distribution of neurons projecting to the rostral ventrolateral medullary pressor region that are activated by sustained hypotension. Neuroscience 89, 1319–1329.

Housley, G.D., Martin-Body, R.L., Dawson, N.J., Sinclair, J.D., 1987. Brain stem projections of the glossopharyngeal nerve and its carotid sinus branch in the rat. Neuroscience 22, 237–250. https://doi.org/10.1177/0964663912467814.

Housley, G.D., Sinclair, J.D., 1988. Localization by kainic acid lesions of neurones transmitting the carotid chemoreceptor stimulus for respiration in rat. J. Physiol. 406, 99–114.

Jee, Y.-S., Ko, I.-G., Sung, Y.-H., Lee, J.-W., Kim, Y.-S., Kim, S.-E., Kim, B.-K., Seo, J.-H., Shin, M.-S., Lee, H.-H., Cho, H.-J., Kim, C.-J., 2008. Effects of treadmill exercise on memory and c-Fos expression in the hippocampus of the rats with intracerebroventricular injection of streptozotocin. Neurosci. Lett. 443, 188–192. https://doi.org/10.1016/j.neulet.2008.07.078.

Kanjhan, R., Lipski, J., Kruszewska, B., Rong, W., 1995. A comparative study of pre-sympathetic and Bötzinger neurons in the rostral ventrolateral medulla (RVLM) of the rat. Brain Res. 699, 19–32.

Kesslak, J.P., Nalcioglu, O., Cotman, C.W., 1991. Quantification of magnetic resonance scans for hippocampal and parahippocampal atrophy in Alzheimer's disease. Neurology 41, 51–54.

King, T.L., Kline, D.D., Ruyle, B.C., Heesch, C.M., Hasser, E.M., 2013. Acute systemic hypoxia activates hypothalamic paraventricular nucleus-projecting catecholaminergic neurons in the caudal ventrolateral medulla. Am. J. Physiol. Regul. Integr. Comp. Physiol. 305, R1112–R1123. https://doi.org/10.1152/ajpregu.00280.2013.

Kraska, A., Santin, M.D., Dorieux, O., Joseph-Mathurin, N., Bourrin, E., Petit, F., Jan, C., Chaigneau, M., Hantraye, P., Lestage, P., Dhenain, M., 2012. In vivo cross-sectional characterization of cerebral alterations induced by intracerebroventricular administration of streptozotocin. PLoS One 7, e46196. https://doi.org/10.1371/journal.pone.0046196.

La Monte, S.D., Wands, J., 2005. Review of insulin and insulin-like growth factor expression, signaling, and malfunction in the central nervous system: relevance to Alzheimer's disease. J. Alzheimers Dis. 7, 45–61.

Lee, J.H., Ryan, J., Andreescu, C., Aizenstein, H., Lim, H.K., 2015. Brainstem morphological changes in Alzheimer's disease. Neuroreport 26, 411–415. https://doi.org/10.1097/WNR.0000000000000362.

Lester-Coll, N., Rivera, E.J., Soscia, S.J., Doiron, K., Wands, J.R., de la Monte, S.M., 2006. Intracerebral streptozotocin model of type 3 diabetes: relevance to sporadic Alzheimer's disease. J. Alzheimers Dis. 9, 13–33.

Mandel, D.A., Schreihofer, A.M., 2009. Modulation of the sympathetic response to acute hypoxia by the caudal ventrolateral medulla in rats. J. Physiol. 587, 461–475. https://doi.org/10.1113/jphysiol.2008.161760.

Marty, V., El Hachmane, M., Amédée, T., 2008. Dual modulation of synaptic transmission in the nucleus tractus solitarius by prostaglandin E2 synthesized downstream of IL-1beta. Eur. J. Neurosci. 27, 3132–3150. https://doi.org/10.1111/j.1460-9568.2008.06296.x.

Monnier, A., Alheid, G.F., McCrimmon, D.R., 2003. Defining ventral medullary respiratory compartments with a glutamate receptor agonist in the rat. J. Physiol. 548, 859–874. https://doi.org/10.1113/jphysiol.2002.038141.

Moraes, D.J.A., Zoccal, D.B., Machado, B.H., 2012. Sympathoexcitation during chemoreflex active expiration is mediated by L-glutamate in the RVLM/Bötzinger complex of rats. J. Neurophysiol. 108, 610–623. https://doi.org/10.1152/jn.00057.2012.

Mutolo, D., Bongianni, F., Nardone, F., Pantaleo, T., 2005. Respiratory responses evoked by blockades of ionotropic glutamate receptors within the Bötzinger complex and the pre-Bötzinger complex of the rabbit. Eur. J. Neurosci. 21, 122–134. https://doi.org/10.1111/j.1460-9568.2004.03850.x.

Nitsch, R., Hoyer, S., 1991. Local action of the diabetogenic drug, streptozotocin, on glucose and energy metabolism in rat brain cortex. Neurosci. Lett. 128, 199–202.

Ostrowski, T.D., Dantzler, H.A., Polo-Parada, L., Kline, D.D., 2017. H2O2 augments cytosolic calcium in nucleus tractus solitarii neurons via multiple voltage-gated calcium channels. Am. J. Physiol. Cell Physiol. 312, C651–C662. https://doi.org/10.1152/ajpcell.00195.2016.

Ostrowski, T.D., Hasser, E.M., Heesch, C.M., Kline, D.D., 2014. $H_2O_2$ induces delayed hyperexcitability in nucleus tractus solitarii neurons. Neuroscience 262, 53–69. https://doi.org/10.1016/j.neuroscience.2013.12.055.

Parvizi, J., Van Hoesen, G.W., Damasio, A., 2001. The selective vulnerability of brainstem nuclei to Alzheimer's disease. Ann. Neurol. 49, 53–66. https://doi.org/10.1002/1531-8249(200101)49:1 < 53::AID-ANA30 > 3.0.CO;2-Q.

Paxinos, G., Watson, C., 2007. The Rat Brain in Stereotaxic Coordinates. Elsevier.

Pickering, M., Cumiskey, D., O'Connor, J.J., 2005. Actions of TNF-alpha on glutamatergic synaptic transmission in the central nervous system. Exp. Physiol. 90, 663–670. https://doi.org/10.1113/expphysiol.2005.030734.

Rai, S., Kamat, P.K., Nath, C., Shukla, R., 2014. Glial activation and post-synaptic neurotoxicity: the key events in streptozotocin (ICV) induced memory impairment in rats. Pharmacol. Biochem. Behav. 117, 104–117. https://doi.org/10.1016/j.pbb.2013.11.035.

Salkovic-Petrisic, M., Knezovic, A., Hoyer, S., Riederer, P., 2013. What have we learned from the streptozotocin-induced animal model of sporadic Alzheimer's disease, about the therapeutic strategies in Alzheimer's research. J. Neural Transm. 120, 233–252. https://doi.org/10.1007/s00702-012-0877-9.

Santos, T.O., Mazucanti, C.H.Y., Xavier, G.F., Torrão, A.S., 2012. Early and late neurodegeneration and memory disruption after intracerebroventricular streptozotocin. Physiol. Behav. 107, 401–413. https://doi.org/10.1016/j.physbeh.2012.06.019.

Schreihofer, A.M., Guyenet, P.G., 2002. The baroreflex and beyond: Control of sympathetic vasomotor tone by gabaergic neurons in the ventrolateral medulla. Clin. Exp. Pharmacol. Physiol. 29, 514–521. https://doi.org/10.1046/j.1440-1681.2002.03665.x.

Sharma, M., Gupta, Y.K., 2001. Intracerebroventricular injection of streptozotocin in rats produces both oxidative stress in the brain and cognitive impairment. Life Sci. 68, 1021–1029.

Shoham, S., Bejar, C., Kovalev, E., Weinstock, M., 2003. Intracerebroventricular injection of streptozotocin causes neurotoxicity to myelin that contributes to spatial memory deficits in rats. Exp. Neurol. 184, 1043–1052. https://doi.org/10.1016/j.expneurol.2003.08.015.

Simic, G., Stani, G., Mladinov, M., Jovanov-Milosevic, N., Hof, P.R., 2010. Does Alzheimer's disease begin in the brainstem. Neuropathol. Appl. Neurobiol. 35, 532–554. https://doi.org/10.1111/j.1365-2990.2009.01038.x.Annotation.

Smith, J.C., Abdala, A.P.L., Borgmann, A., Rybak, I.A., Paton, J.F.R., 2013. Brainstem respiratory networks: building blocks and microcircuits. Trends Neurosci. 36, 152–162. https://doi.org/10.1016/j.tins.2012.11.004.

Teppema, L.J., Veening, J.G., Kranenburg, A., Dahan, A., Berkenbosch, A., Olievier, C., 1997. Expression of c-fos in the rat brainstem after exposure to hypoxia and to normoxic and hyperoxic hypercapnia. J. Comp. Neurol. 388, 169–90. https://doi.org/10.1002/(SICI)1096-9861(19971117)388:2 < 169::AID-CNE1 > 3.0.CO;2-#.

Thévenaz, P., Unser, M., 2007. User-friendly semiautomated assembly of accurate image mosaics in microscopy. Microsc. Res. Tech. 70, 135–146. https://doi.org/10.1002/jemt.20393.

Verberne, A.J.M., Stornetta, R.L., Guyenet, P.G., 1999. Properties of C1 and other ventrolateral medullary neurones with hypothalamic projections in the rat. J. Physiol. 517 (Pt 2), 477–494. https://doi.org/10.1111/j.1469-7793.1999.0477t.x.

Wang, X., Guo, R., Zhao, W., 2015. Distribution of fos-like immunoreactivity, catecholaminergic and serotoninergic neurons activated by the laryngeal chemoreflex in the medulla oblongata of rats. PLoS One 10, e0130822. https://doi.org/10.1371/journal.pone.0130822.

Wang, H., Stornetta, R.L., Rosin, D.L., Guyenet, P.G., 2001. Neurokinin-1 receptor-immunoreactive neurons of the ventral respiratory group in the rat. J. Comp. Neurol. 434, 128–146.

Zimny, A., Bladowska, J., Neska, M., Petryszyn, K., Guziński, M., Szewczyk, P., Leszek, J., Sąsiadek, M., 2013. Quantitative MR evaluation of atrophy, as well as perfusion and diffusion alterations within hippocampi in patients with Alzheimer's disease and mild cognitive impairment. Med. Sci. Monit. 19, 86–94. https://doi.org/10.12659/msm.883757.